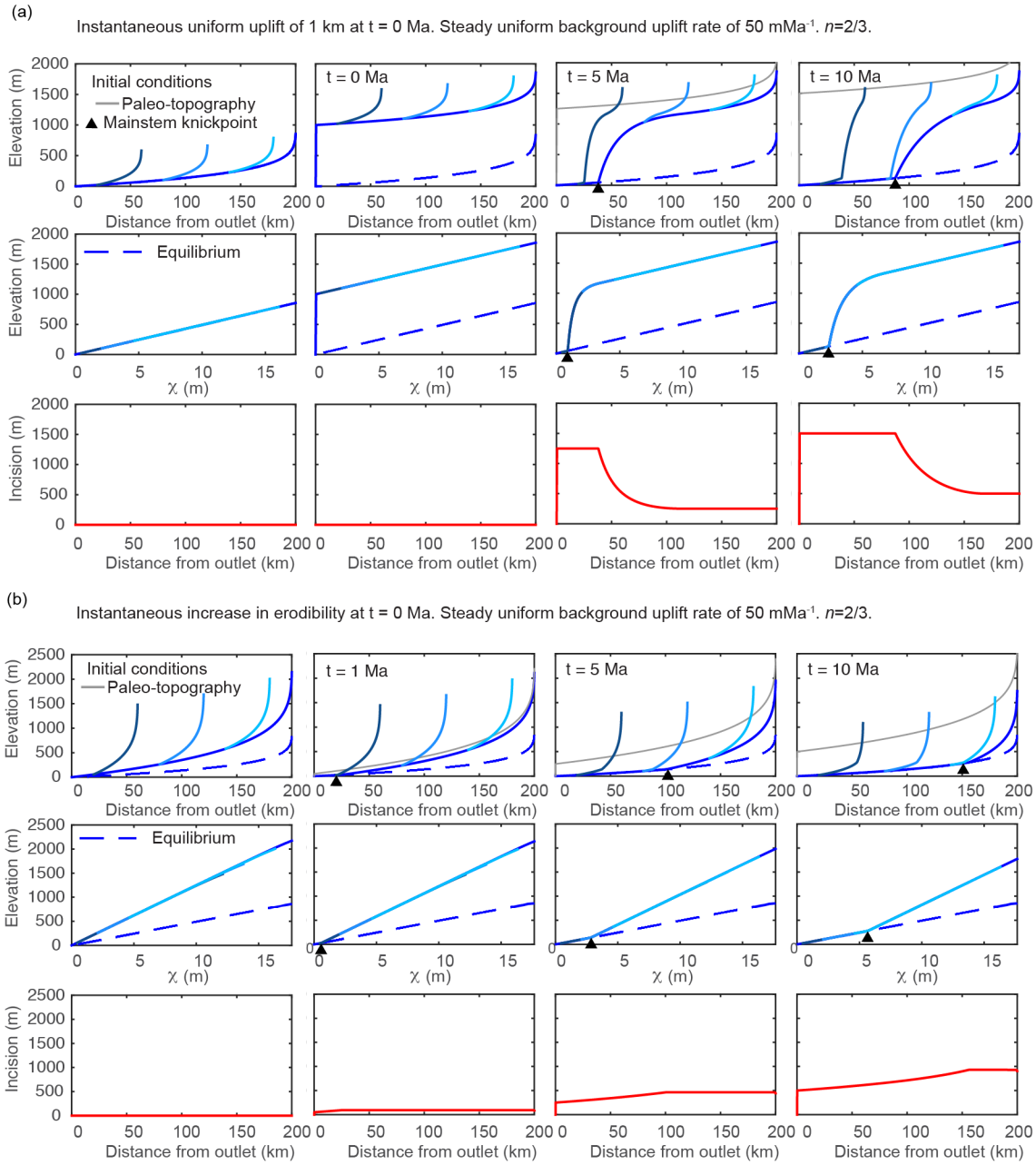

Figure S1. Results from 1-D simulations of equilibrated river network subject to various perturbations that move profiles away from equilibrium. Simulations are analogous to those presented in Fig. 2 but were run with $n = 2/3$. We used the same concavity, $\theta = 0.45$, as other simulations but adjusted K to 3.7×10^{-6} $\mathrm{m}^{0.4}\mathrm{yr}^{-1}$ such that steady-state fluvial relief remained the same between all simulations run with $n = 1$ and $n = 2/3$. Results from multiple timesteps for simulation of instantaneous uniform uplift of: 1 km at $t = 0$ Ma (**a**); step increase in erodibility, K, or equivalently a step decrease in rock uplift rate (**b**). Line color, basic description of plots filling each row, and network structure are the same as described in Fig. 2.

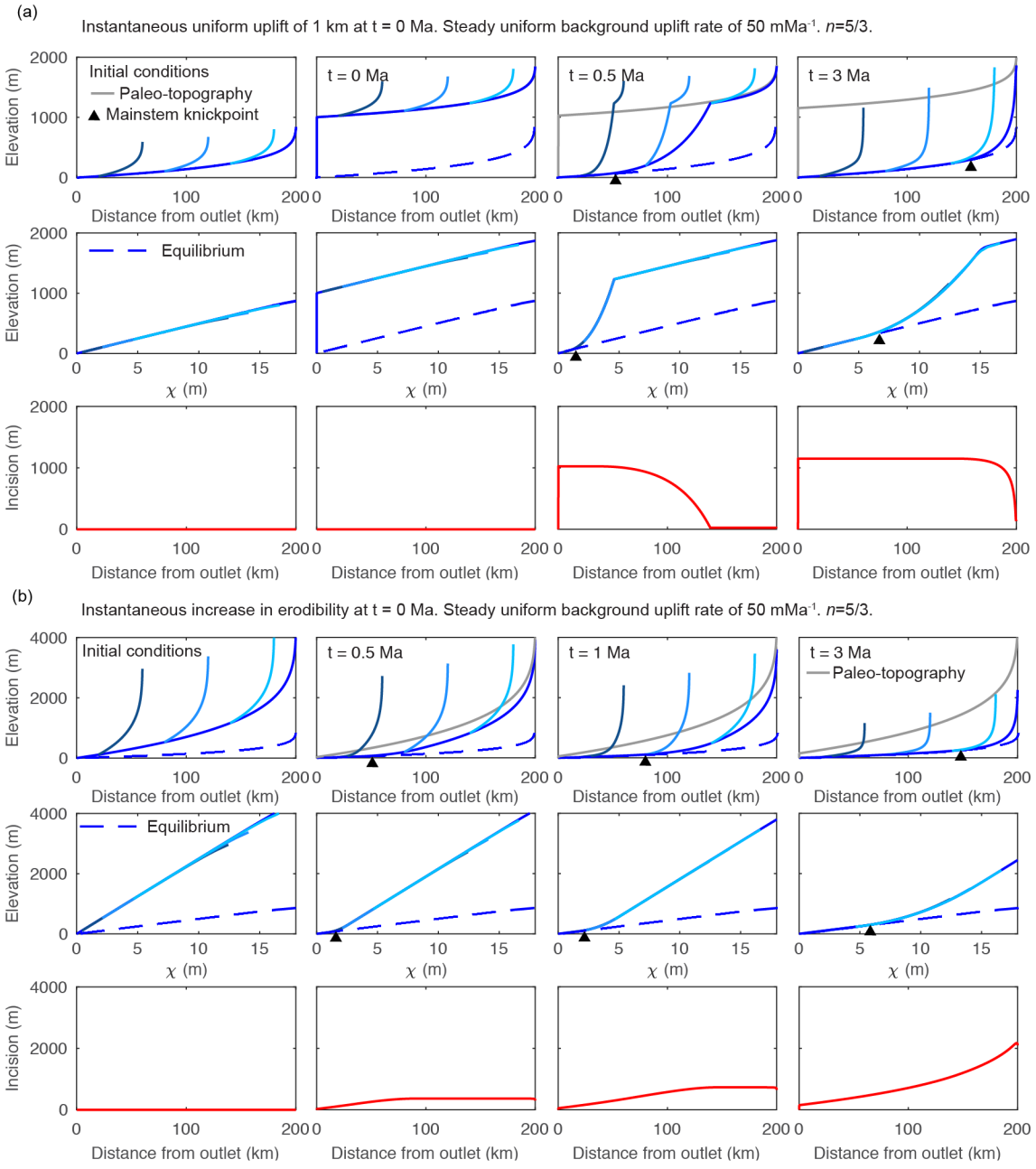

Figure S2. Results from 1-D simulations of equilibrated river network subject to various perturbations that move profiles away from equilibrium. Simulations are analogous to those presented in Fig. 2 but were run with $n = 5/3$. We used the same concavity, $\theta = 0.45$, as other simulations but adjusted K to 7.4×10^{-8} $\mathrm{m}^{-0.5}\mathrm{yr}^{-1}$ such that steady-state fluvial relief remained the same between all simulations run with $n = 1$ and $n = 5/3$. Results from multiple timesteps for simulation of instantaneous uniform uplift of: 1 km at t=0 Ma (**a**); step increase in erodibility, K (**b**). Line color, basic description of plots filling each row, and network structure are the same as described in Fig. 2.

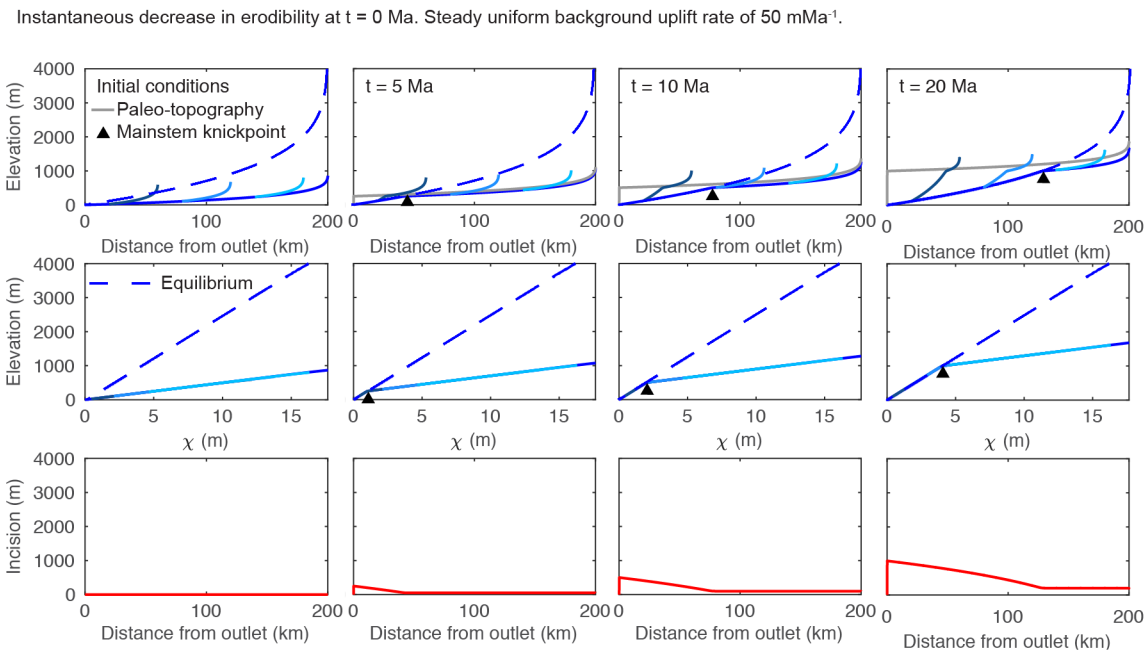

Figure S3. Results from multiple timesteps for simulation of a step decrease in erodibility, K. The initial condition is a river profile equilibrated to a uniform background uplift rate of 50 mMa^{-1} and a erodibility of $K = 1\times10^{-6}$ $\mathrm{m}^{0.1}\mathrm{yr}^{-1}$, which is then lowered to $K = 2\times10^{-7}$ $\mathrm{m}^{0.1}\mathrm{yr}^{-1}$. An increase in uplift rate from 50 to 250 mMa^{-1} produces the same profile form but with faster response times. Line color, basic description of plots filling each row, and network structure are the same as described in Fig. 2.

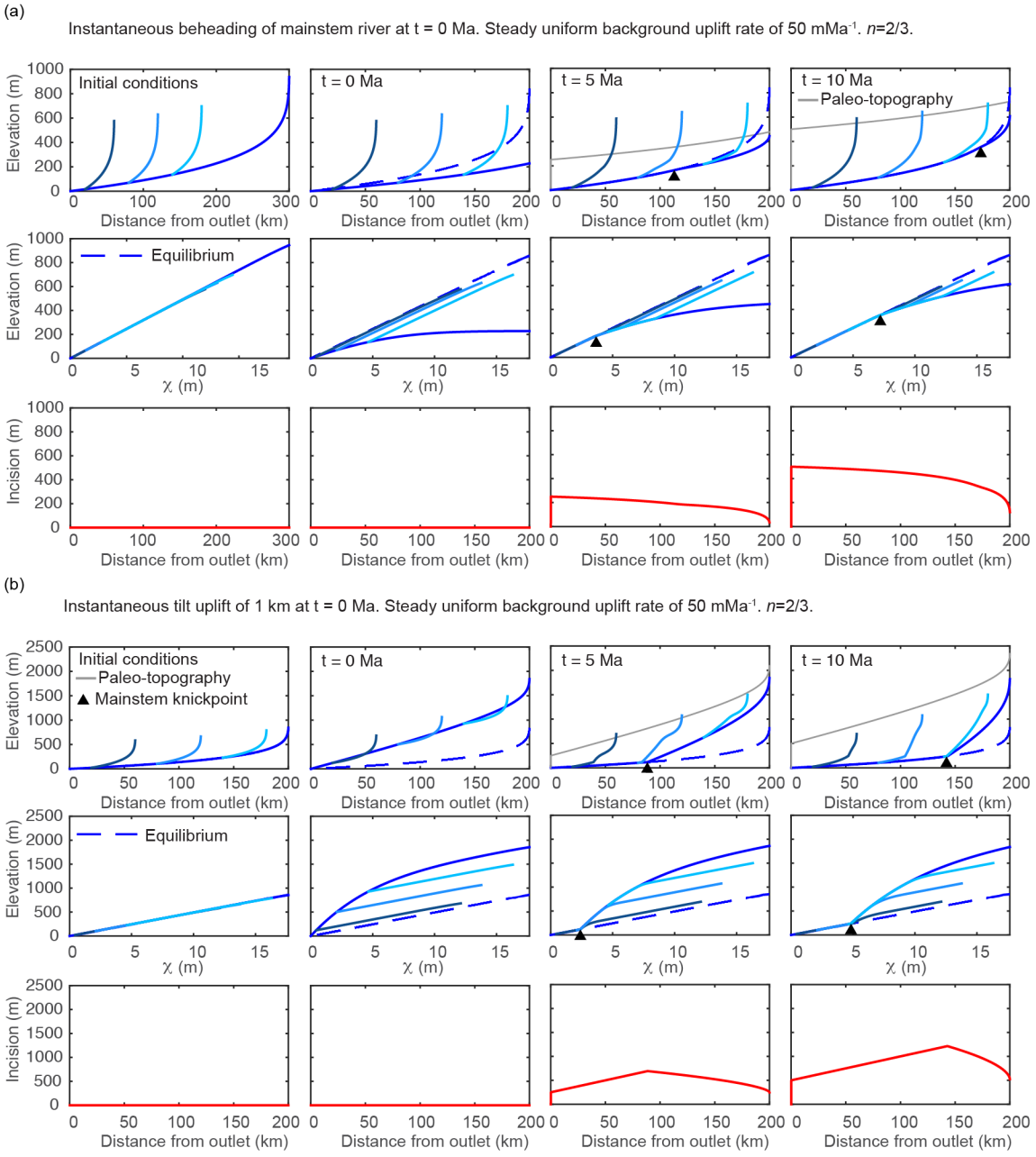

Figure S4. Results from 1-D simulations of equilibrated river network subject to various perturbations that move profiles away from equilibrium. Simulations are analogous to those presented in Fig. 3 but were run with $n = 2/3$. We used the same concavity, $\theta = 0.45$, as other simulations but adjusted K to 3.7×10^{-6} $\mathrm{m}^{0.4}\mathrm{yr}^{-1}$ such that steady-state fluvial relief remained the same between all simulations run with $n = 1$ and $n = 2/3$. Results from multiple timesteps for simulation of instantaneous truncation of a 300 km long river to from a 200 km long river (**a**); and instantaneous tilting at $t = 0$ Ma with tilt axis at the river mouth, perpendicular to the main stem, and 1 km maximum uplift at the channel head (**b**). Line color, basic description of plots filling each row, and network structure are the same as described in Fig. 2.

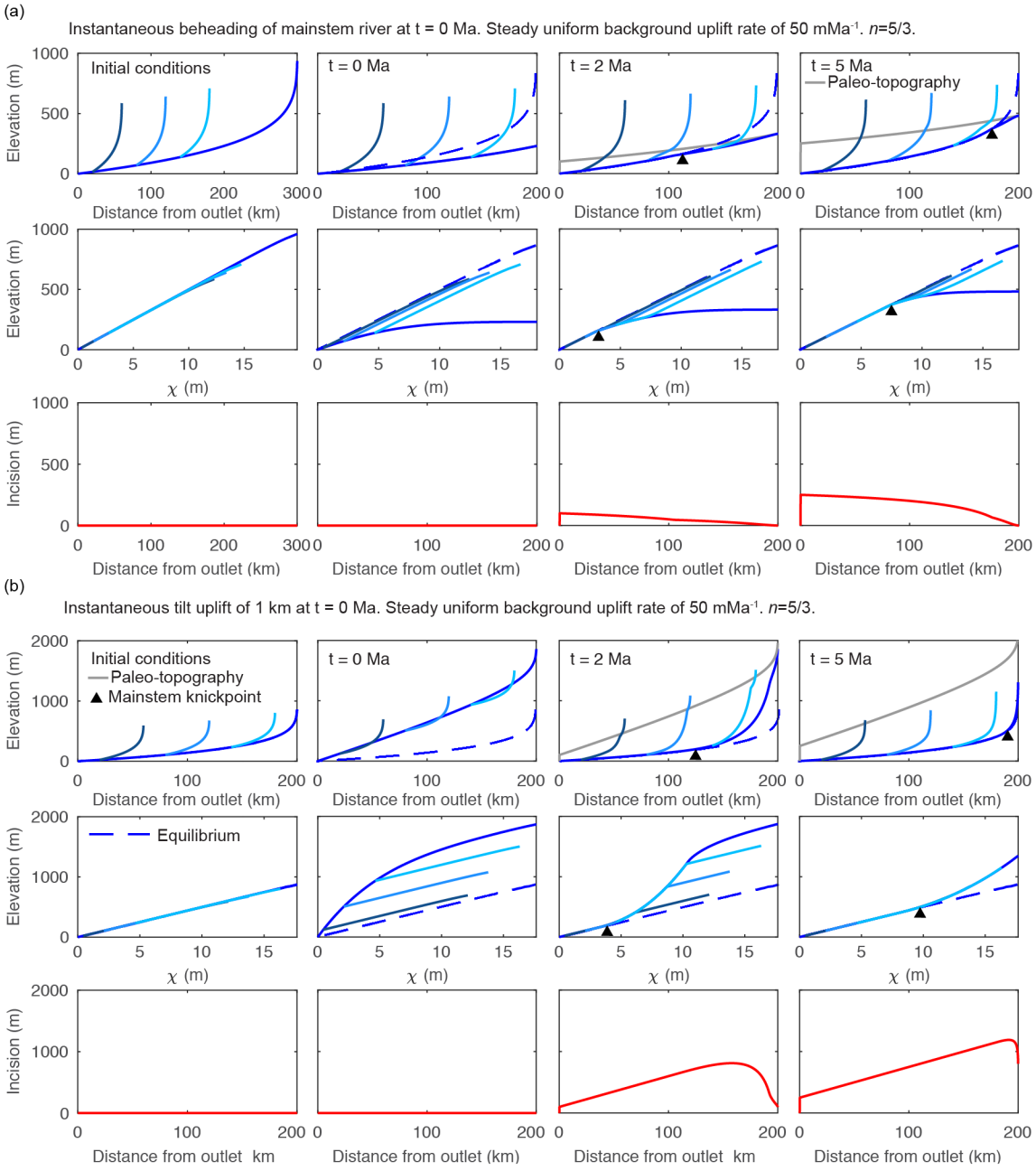

Figure S5. Results from 1-D simulations of equilibrated river network subject to various perturbations that move profiles away from equilibrium. Simulations are analogous to those presented in Fig. 3 but were run with $n = 5/3$. We used the same concavity, $\theta = 0.45$, as other simulations but adjusted K to 7.4×10^{-8} $\mathrm{m}^{-0.5}\mathrm{yr}^{-1}$ such that steady-state fluvial relief remained the same between all simulations run with $n = 1$ and $n = 5/3$. Results from multiple timesteps for simulation of instantaneous truncation of a 300 km long river to from a 200 km long river (**a**); and instantaneous tilting at $t = 0$ Ma with tilt axis at the river mouth, perpendicular to the main stem, and 1 km maximum uplift at the channel head (**b**). Line color, basic description of plots filling each row, and network structure are the same as described in Fig. 2.

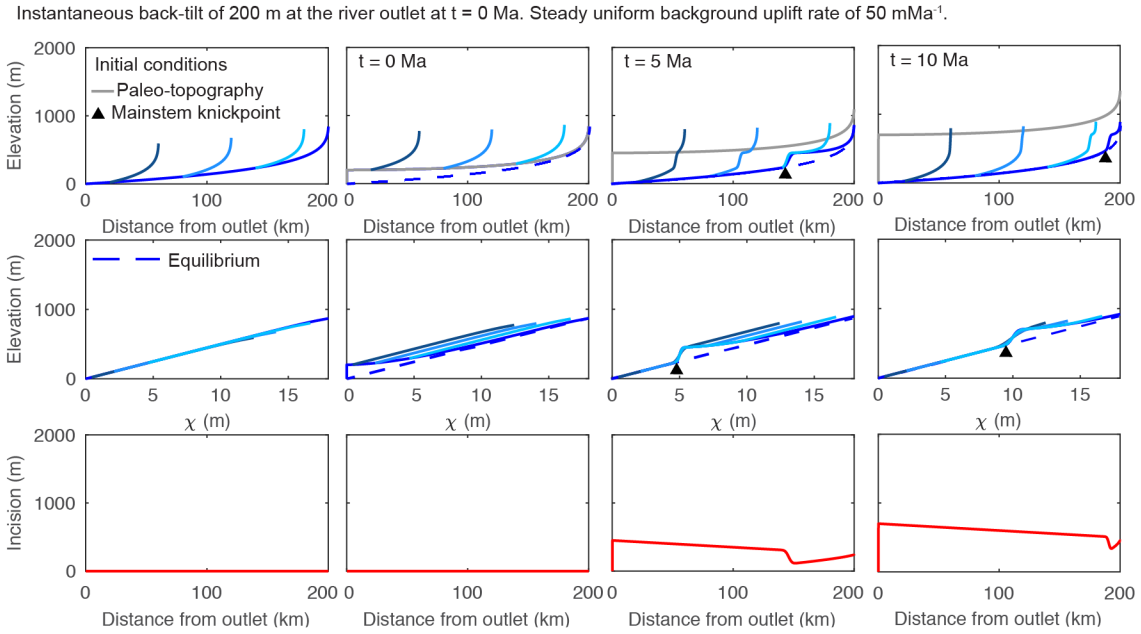

Figure S6. Results from 1-D simulations of equilibrated river network subject to various perturbations that move profiles away from equilibrium. Results from multiple timesteps for simulation of instantaneous lateral tilt of 1 km about an axis located on the mainstem and perpendicular to the tributaries. Line color, basic description of plots filling each row, and network structure are the same as described in Fig. 2.

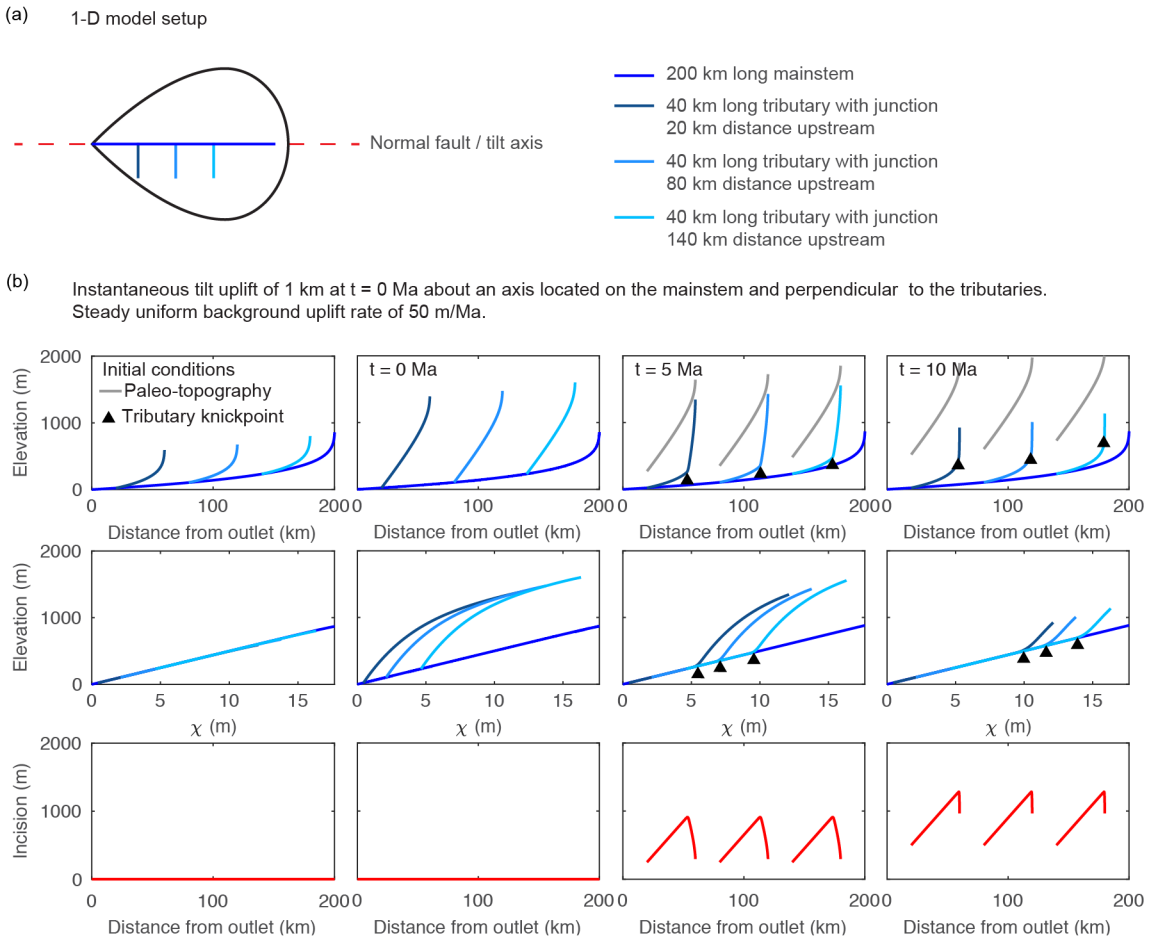

Figure S7. Results from 1-D simulations of equilibrated river network subject to various perturbations that move profiles away from equilibrium. (**a**) 1-D model setup for simulation of instantaneous lateral tilt of a drainage basin. (**b**) Results from multiple timesteps for simulation of instantaneous lateral tilt of 1 km about an axis located on the mainstem and perpendicular to the tributaries. Basic description of plots filling each row are the same as described in Fig. 2.

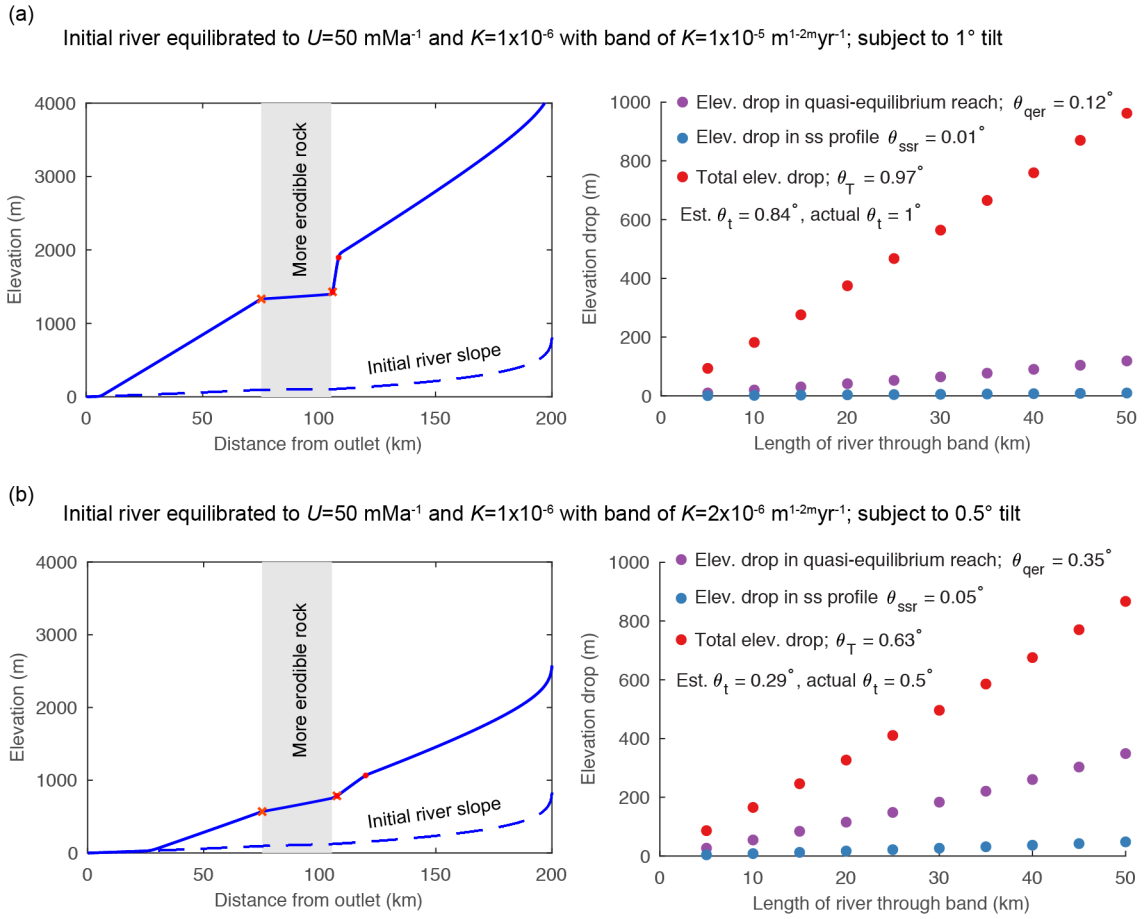

Figure S8. Measurements of tilt angle from the geometry of mid-profile knickzones in a 1-D model of instantaneous tilt of 1° at $t = 0$ with bands of soft rock of increasing width at 75 km upstream in a 200 km river. Erodibility in the band of soft rock is a factor of two greater ($K = 2 \times 10^{-6}$ $\mathrm{m}^{0.1}\mathrm{yr}^{-1}$) than the rest of profile ($K = 1 \times 10^{-6}$ $\mathrm{m}^{0.1}\mathrm{yr}^{-1}$). Initial river profile is equilibrated to $K = 1 \times 10^{-6}$ $\mathrm{m}^{0.1}\mathrm{yr}^{-1}$. (**a**) and (**b**) Examples of river profiles at the end of simulations for the case in which the base of the knickzone is at the upper rock-type contact (**a**) as compared to the case in which the base of the knickzone has propagated 5 km upstream of the upper rock-type contact (**b**). In each simulation, the knickzone is identified using peaks and troughs in curvature of the river profile. (**c**) and (**d**) Measurements of knickzone height as a function of length of reach with more erodible rock. Simulations were stopped and measurements of knickzone height were taken when the base of the knickzone was at the upper lithologic contact (**c**) and 5 km upstream of upper contact (**d**). Tilt angle is estimated using linear regression of knickzone height measurements with the intercept forced through the origin.

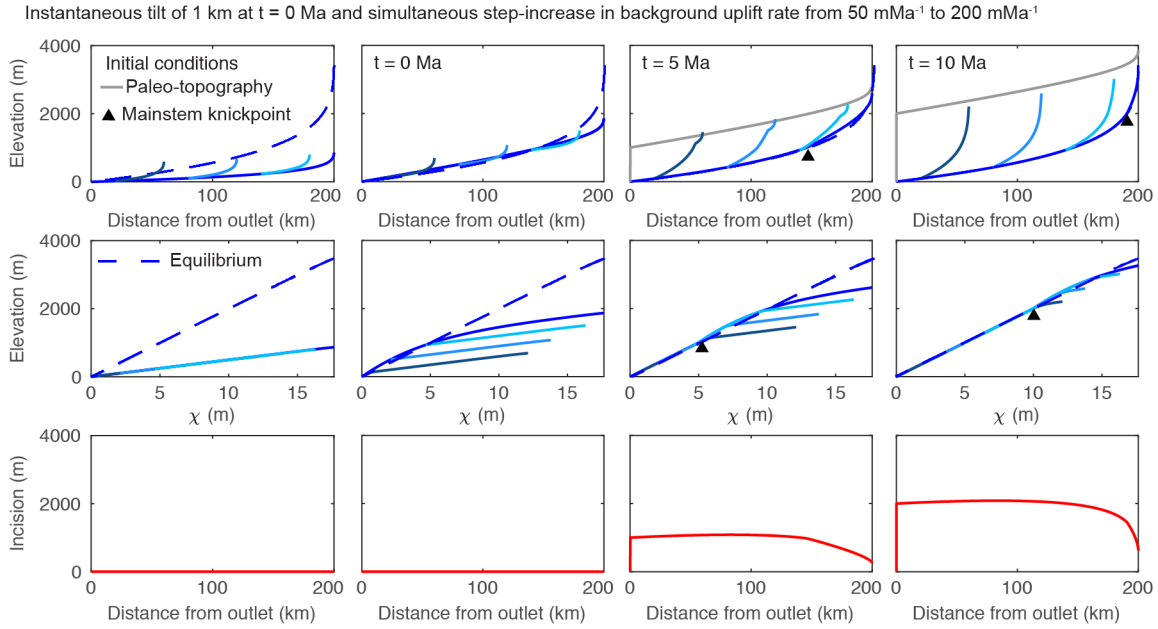

Figure S9. Results from multiple timesteps for simulation of instantaneous tilting at $t = 0$ Ma with a simultaneous step-increase in background uplift rate from 50 mMa^{-1} to 200 mMa^{-1}. The initial condition is a river profile equilibrated to a uniform background uplift rate of 50 mMa^{-1} and a erodibility of $K = 1 \times 10^{-6}$ $\mathrm{m}^{0.1}\mathrm{yr}^{-1}$. Line color, basic description of plots filling each row, and network structure are the same as described in Fig. 2.

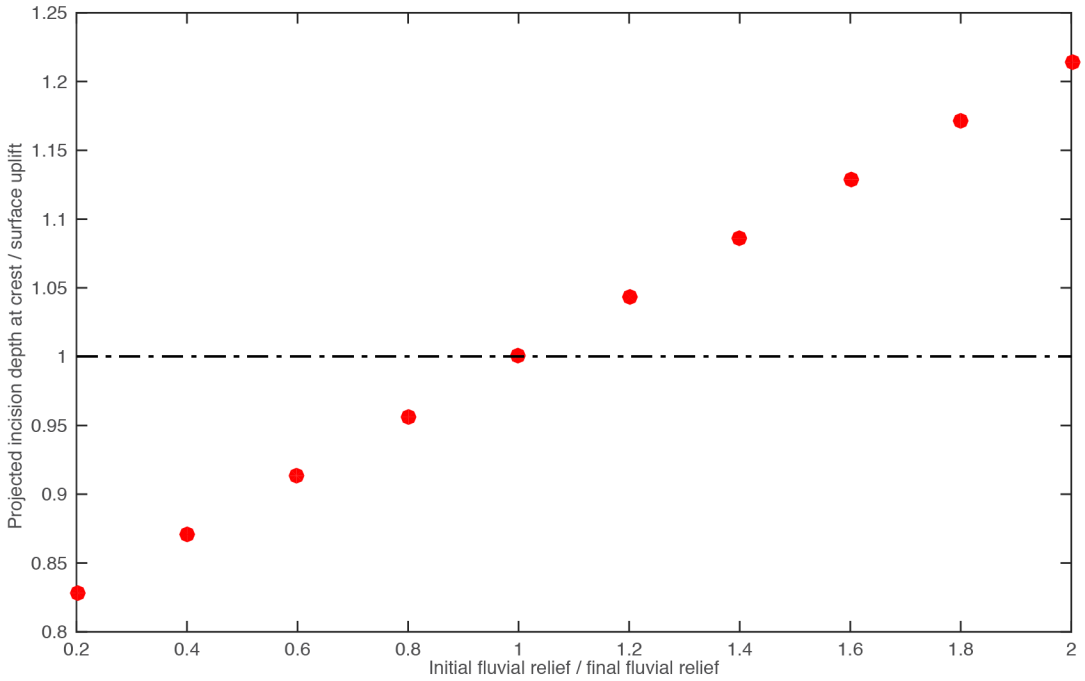

Figure S10. Estimates of surface uplift made from incision depth below paleotopography markers from 1-D simulations of a rapid pulse of nonuniform uplift due to tilting accompanied by a step-change in fluvial relief.

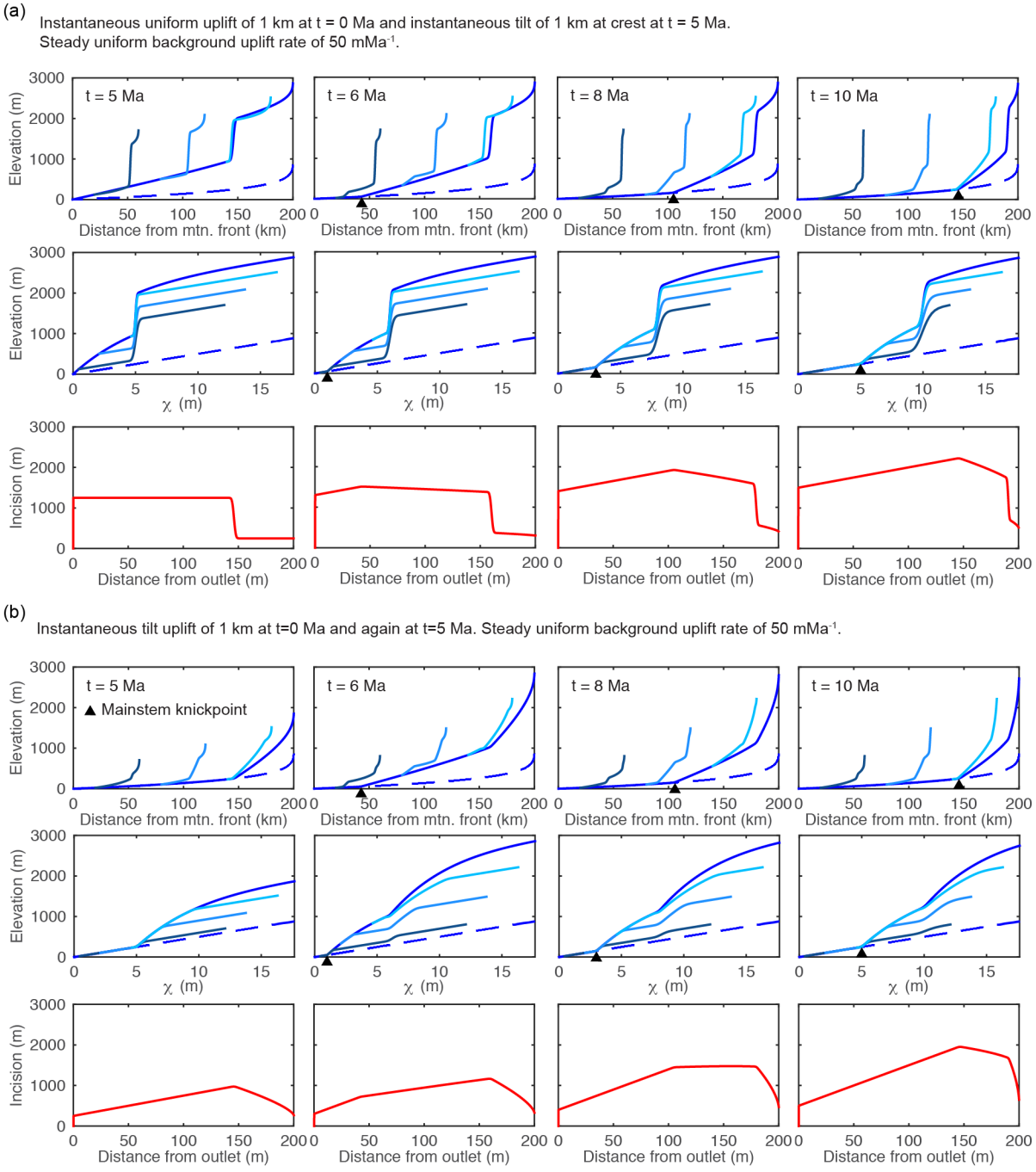

Figure S11. Results from 1-D river simulations of rapid nonuniform uplift due to tilting with disequilibrium initial conditions. (**a**) Uniform pulse of uplift of 1 km at $t = 0$ Ma and instantaneous tilt of 1 km at the crest at $t = 5$ Ma. (**b**) Instantaneous tilt of 1 km at $t = 0$ Ma and a an instantaneous tilt of 1 km at $t = 5$ Ma. Line color, basic description of plots filling each row, and network structure are the same as described in Fig. 2.